Castro-Chacón, Andres ; Castro-Carranza, Alejandra ; Amargós-Reyes, Olivia ; Maldonado, José-Luis ; Hernández-Cristóbal, Orlando ; Guzmán-Caballero, David ; Mejía, Israel ; Vázquez, Aldo ; Gutowski, Jürgen ; Nolasco, Jairo C.

Relationship between the VOC Tuning Effect and the Interface Activation Energy Due to the Third Component Concentration in Ternary Organic Solar Cells

Journal Article as: peer-reviewed accepted version (Postprint)

DOI of this document*(secondary publication): https://doi.org/10.26092/elib/3717

Publication date of this document: 21/02/2025

* for better findability or for reliable citation

Recommended Citation (primary publication/Version of Record) incl. DOI:

Relationship between the VOC Tuning Effect and the Interface Activation Energy Due to the Third Component Concentration in Ternary Organic Solar Cells. Andres Castro-Chacón, Alejandra Castro-Carranza, Olivia Amargós-Reyes, José-Luis Maldonado, Orlando Hernández-Cristóbal, David Guzmán-Caballero, Israel Mejía, Aldo Vázquez, Jürgen Gutowski, and Jairo C. Nolasco. ACS Applied Energy Materials 2022 5 (4), 4288-4295
DOI: 10.1021/acsaem.1c03888

Relationship between the V_{OC} Tuning Effect and the Interface Activation Energy due to the Third Component Concentration in Ternary Organic Solar Cells

*Andres Castro-Chacón[†], Alejandra Castro-Carranza[†, ‡], Olivia Amargós-Reyes[§], José-Luis Maldonado[§], Orlando Hernández-Cristóbal[¶], David Guzmán-Caballero[¥], Israel Mejía[¥], Aldo Vázquez[#], Jürgen Gutowski[#, ǁ], Jairo C. Nolasco[#, *]*

[†] International Laboratory of Environmental Electron Devices (LAIDEA UNAM), ENES Morelia, National Autonomous University of Mexico, 58190 Morelia, Mexico.

[‡] Semiconductor Optics, Institute of Solid-State Physics, University of Bremen, 28359 Bremen, Germany.

[§] Research Group of Optical Properties of Materials (GPOM) Centro de Investigaciones en Óptica A.C. A.P. 1-948, 37150 León, Gto., Mexico.

[¶]Laboratory of Microscopy, National School of Higher Studies, ENES Morelia, National Autonomous University of Mexico, 58190 Morelia, Mexico.

[¥]Center for Engineering and Industrial Development, CIDESI, Division of Microtechnologies, 76125, Santiago de Querétaro, Querétaro, Mexico.

[‖] MAPEX Center of Materials and Processes, University of Bremen, 28359 Bremen, Germany.

[#] Micro and Nanotechnology Research Center (MICRONA), Veracruz University, Boca del Río, Veracruz 94294, México.

ABSTRACT

The open circuit voltage (V_{OC}) tuning effect due to the variation of the low concentration of the third component in ternary organic solar cells has been mainly attributed to interfacial phenomena. Up to date, the models reported in literature to analyze such interfacial phenomena are based on optical characterization. In this work is proposed a different approach to study such V_{OC} tunning effect by using dark-current characteristics at different temperatures. Specifically, for PTB7-Th:PC_{71}BM:ICBA based solar cells, it is found that an increment of the third component concentration, i.e. the fullerene ICBA, causes an increase of the activation energies (E_a) in an Arrhenius type curves. This in turn decreases the reverse saturation current (J_0) of the devices, thereby incrementing their V_{OC}.

KEY WORDS: Ternary organic solar cells, open circuit voltage, activation energy, third material effect, low concentration, dark current characteristics, interfacial effect.

TOC Graphic

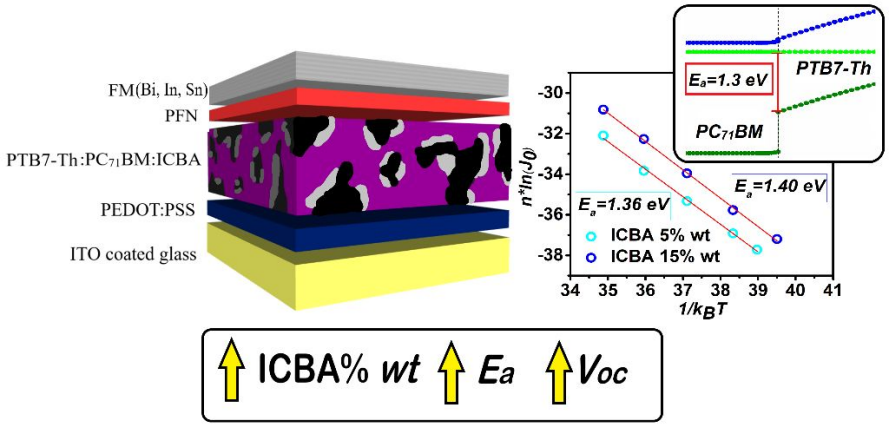

INTRODUCTION

Organic photovoltaic devices (OPVs) offer nowadays an important and potentially cheap option for the generation of clean and renewable energy. This is due to the use of carbon-based materials, such as small molecules and polymers, flexible devices, and the low-cost manufacturing processes

in comparison with conventional silicon-based solar cells [1]. However, for a substantial commercialization of this technology it is necessary to improve the photovoltaic characteristics of such devices to enhance the power conversion efficiency (PCE), which recently have achieved 18.4% and 19% for binary and ternary devices respectively [2, 3].

The latest research in the field of OPVs is mainly concerned with costly novel non-fullerene solar cells [4, 5, 6]. Whereas a strategy to increase light harvesting, while maintaining the simplicity of the organic bulk heterojunction solar cells, i. e. one single deposition step, is focusing on organic ternary solar cells (TSCs) [7-10]. Typically, TSCs are characterized by the introduction of a third component with a low-concentration into a base donor:acceptor bulk heterojunction. Such a third component can be a donor or acceptor material. Depending on its concentration, location, and energy levels with respect to the main heterojunction, it is possible to modify the electronic transport within the device [11]. Ideally, the third compound should be located at the interface of the main heterojunction with the aim to avoid charge recombination and thus, to simultaneously, increase: the short circuit current (J_{SC}), the open circuit voltage (V_{OC}), and the fill factor (FF). Particularly, the origin of the V_{OC} increment has been a topic of intense research [12-17].

The observed dependence of V_{OC} on the concentration of the third component has been attributed to either the heterojunction interface or to bulk recombination [12-17]. For low third component concentrations, the V_{OC} variation has been usually attributed to an interfacial effect [18-19]. This phenomenon has been usually studied using optical methods such as photoluminescence and absorbance to calculate interfacial energies [20, 21, 22]. However, such interfacial energies or charge-transfer states are difficult to detect using conventional techniques relying on transmission and reflection measurements [22] and are applied to the main junction of the device without contacts, which in some cases can determine its V_{OC} [23]. In the present study, it is shown for the first time that the typically observed V_{OC} tuning effect in TSCs with a low third-component concentration can be understood using a simple electrical characterization, i. e., the thermal analysis of current density-voltage (*J-V*) characteristics of the complete device under dark conditions.

Specifically, in this work, we study TCSs based on a PTB7-Th:$PC_{71}BM$ blend with two different but low ICBA concentrations of 5% wt and 15% wt. First, the V_{OC} is calculated using J-V curves in dark and a general model to verify that V_{OC} is determined by the inverse saturation current (J_0).

Then, a dark *J-V* characterization with the temperature as parameter (*J-V-T*) is performed in order to study the dependence of J_0 and the ideality factor on *T*. With this parameter, the activation energies E_a for each device is being calculated using an Arrhenius modified curve. Finally, we compare our calculated activation energies with other parameter values reported in literature.

MATERIALS AND METHODS

Device Fabrication.

Glass substrates coated with indium tin oxide (ITO) (10 Ω/sq, ~165 nm thickness from Delta Technologies) are cut (~1.8 cm × 1.8 cm) and consecutively ultrasonically cleaned for about 20 min in a detergent solution, distilled water, and ethanol. Then, they are dried in an oven at 80 ˚C for at least 12 h. Afterwards, ITO substrates are treated with oxygen plasma for 15 min. A poly(3,4-ethylene- dioxythiophene): poly(styrenesulfonate) (PEDOT:PSS) (Heraeus Clevios PVP AI 4083) layer of 40-nm thickness is spin-coated at 4500 rpm on top of the ITO substrate and annealed in an oven for 20 minutes at 120 ˚C. PTB7-Th (Poly [[4,8-bis[(2-ethylhexyl)oxy] benzo[1,2-b:4,5-b']dithiophene-2,6-diyl] [3-fluoro-2-[(2-ethylhexyl) carbonyl]thieno [3,4-b]thiophenediyl]], 1-Material Inc.) is used as an electron donor semiconductor. Both [6,6]-phenyl-C_{71}-butyric acid

methyl ester ($PC_{71}BM$) and indene-C60 bisadduct (ICBA) (1-Material Inc.) served as electron acceptors.

The solution for the active layer is prepared by dissolving PTB7-Th and $PC_{71}BM$ (1:1.5 w/w, 30 mg/ml in anhydrous chlorobenzene/1,8-diiodooctane (97:3 v/v)) under nitrogen atmosphere. The solution is stirred for about 24 h at room temperature. The ICBA solution is prepared as 10 mg/ml in anhydrous chlorobenzene. Either 5wt% or 15wt% of ICBA with respect to the first acceptor material $PC_{71}BM$ is added to the PTB7-Th:$PC_{71}BM$ solution and stirred for 15 min. Then, the whole solution is spin-coated at normal room temperature and ambient pressure, with a spin velocities of 2200 rpm onto the PEDOT:PSS layer to obtain an active layer thickness of ~100 nm. Thermal annealing of 80 ˚C for 15 minutes is applied to the deposited films. A poly [(9,9-bis(3'-(N,N-dimethylamino)propyl)-2,7-fluorene)-alt-2,7-(9,9–dioctylfluorene)] (PFN) layer (~5-10 nm) is spin-coated at 5500 rpm on top of the active layer and exposed to thermal annealing for 15 minutes at 80 ˚C. Active areas (0.07 cm^2) are delimited with a mask. Fields metal (FM) is an alternative top electrode composed of Bi, Sn and In, previously reported by our group [23, 24, 25]. FM is deposited (after melting it at 95 ˚C in a hot plate) by drop casting on top of the PFN layer.

Finally, OPVs cells are cooled down at room temperature. The TSC's structure as comprising of glass (1.1 mm)/ITO(165 nm)/PEDOT:PSS(40 nm)/PTB7-Th:$PC_{71}BM$:ICBA (~100 nm)/PFN(~5 nm)/FM is illustrated in Figure 1(b). The surface morphology and thicknesses of the films are observed using an atomic force microscope (AFM, easyscan2 from Nanosurf). UV-Vis spectrometer (Lambda 900, Perkin Elmer Instruments) is used to carried out the absorption characterization.

Electrical characterization.

Current density-voltage (*J-V*) characteristics are measured using a Keithley 2400 digital source meter. The *J-V* characteristics under illumination are obtained by using a solar simulator class AAA (Sciencetech SS150) to provide AM1.5 conditions, being calibrated using a silicon reference cell acquired from Abet Technologies. For the analysis at different temperatures, it is used an experimental setup based on an iron plate heated by Nichrome resistors. The samples are heated on the plate, which is properly isolated to reach constant temperatures. The samples were sealed with a temperature resistant tape which protects them from oxygen and moisture. The temperature

is being measured by a thermocouple fixed next to the sample. The thermocouple is connected to a digital thermometer STEREN HER 425.

RESULTS AND DISCUSSION

PTB7-Th:$PC_{71}BM$:ICBA based solar cells are chosen to carry out this study since it is a well-studied configuration for both binary and ternary devices [26, 27, 28].

The experiment performed here basically consist in TSCs samples with a variation of the ICBA concentration in the blend i. e. 5% wt. or 15% wt., which are within the range of values where the photovoltaic parameters are enhanced, as reported in literature (PCEs from 7.35% to 8.24% [29]. Fig.1(a) shows the *J-V* characteristics under illumination of the TSCs with both 5% wt. or 15% wt. ICBA concentrations. A scheme of the device structure is also shown in Fig.1(b) The corresponding photovoltaic parameters are summarized in Table 1.

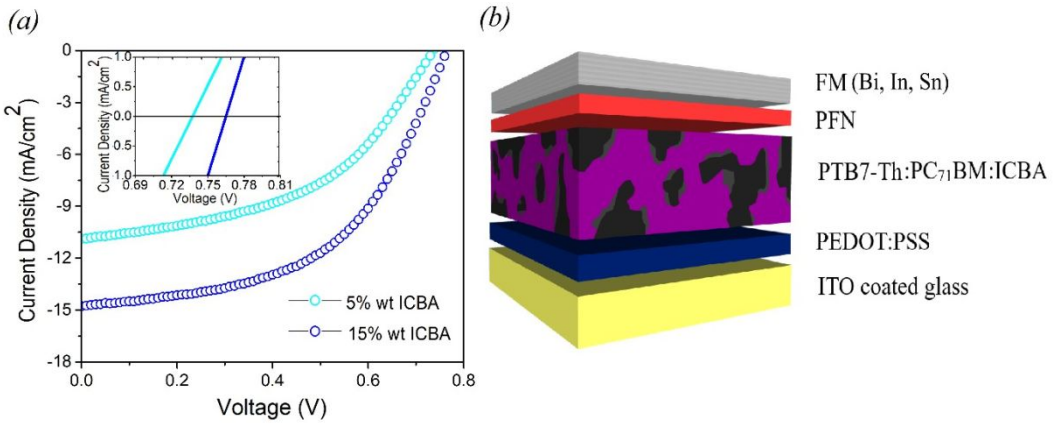

Figure 1. (a) *J-V* characteristics under illumination for TSC's with both 5% wt. or 15% wt. ICBA concentrations. The inset is showing a zoom in of the increment of the V_{OC} got by increasing the ICBA concentration in the ternary blend. (b) TSCs device structure where ICBA domains are shown to be at the interfaces between the main donor:acceptor interface.

Table 1. Photovoltaics parameters under illumination of TSCs with both 5% wt or 15% wt ICBA concentrations.

ICBA % wt	J_{SC} *(mA/cm²)*	V_{OC} *(V)*	*FF*	η *(%)*
5	10.88	0.72	0.47	3.82
15	14.77	0.75	0.52	5.89

Hero devices among 30 samples with a general PCE's standard deviation of around ± 0.4 %.

In Fig.1(a) and Table I, note that at an ICBA concentration of 15% wt all photovoltaic parameters increase regarding to the 5% wt achieving an efficiency of 5.89%, well according to that reported in literature [29, 30]. A mask as often applied to avoid light pipping effects [31] is not used. If a variation of the J-V characteristics under illumination would occur due to such effects, it is expected to affect both devices with different ICBA concentrations equally. Thus, pipping effects should not play a role in the present analysis. The reported efficiencies of devices with similar active materials are slightly higher (~7%) compared with the values obtained for the devices presented within this study. The reason of such differences can be attributed to the use of FM, which is a non-evaporated cathode [24]. This cathode has resulted to be reliable not only to fabricate relatively good devices, but to study charge recombination phenomena occurring in organic solar cells [17]. For more information about this alternative cathode, interface contact, performance, etc. see references [32, 33] The FF is the parameter that limits the efficiency of the herein reported devices in comparison with those reported on in the literature; however, it does not play any role in our analysis, which is focused on V_{OC}. Specifically, a V_{OC} variation of 20 mV to 30 mV for the used third component concentrations is consistent with that reported in literature for

the same acceptor blend [34] and also for systems with different third component (IT-M) but same concentration [35].

To understand the origin of the improvement of the photovoltaic parameters, atomic force microscopy (AFM) characterization and absorbance spectroscopy were performed. Figs. 2 (a) and (b) gained by using AFM show the surface morphologies of the ternary active layers deposited on ITO-coated glass/PEDOT:PSS substrates under the same conditions as in the solar cells. The obtained root-mean-square (RMS) surface roughness is 2 nm and 1.9 nm for samples with 5 % wt. and 15 % wt. ICBA concentration, respectively. The slight decrease of the roughness for the higher ICBA concentration is in good agreement with literature [36, 37, 12, 30]. This trend can be attributed to a denser morphology, i. e., to a higher interpenetration of the material domains [36], which can explain the enhancement of J_{SC} and FF due an improvement of generation, separation, and collection of charges [38]. Further, in Fig.2(c), the absorption coefficient for samples with both 5 % wt. and 15 % wt. ICBA concentrations is depicted. The absorption peaks at about 470 nm, 650 nm, and 740 nm [36] being typical for PTB7-Th are clearly observable.

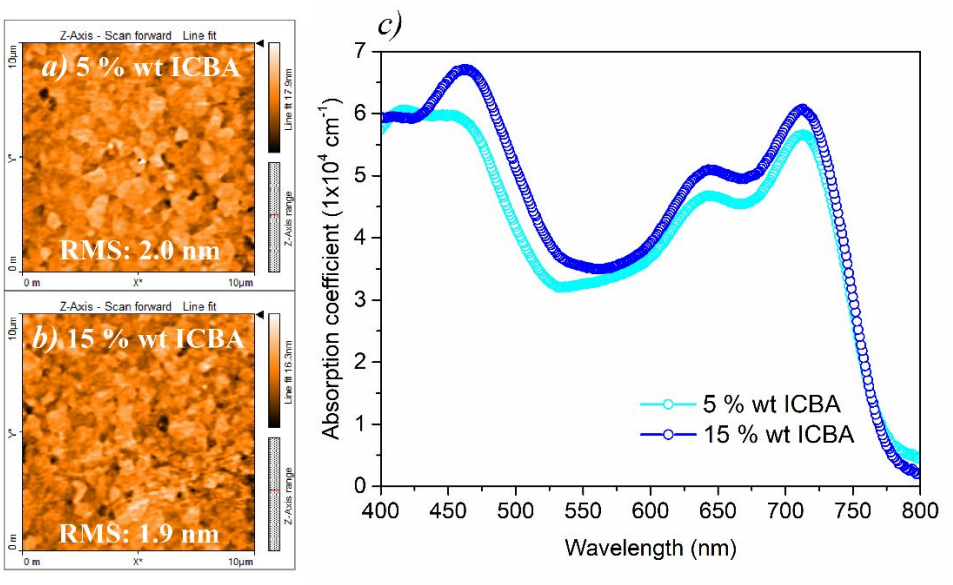

Figure 2. Left: AFM height images of PTB7-Th:$PC_{71}BM$:ICBA active layers with (a) 5 % wt. and (b) 15 % wt. ICBA concentration. The RMS values are specified respectively as inset. Right: (c) Absorption coefficient of the same active layers

The absorption of fullerenes usually increases abruptly below 350 nm (this range is not shown in the figure). A slight increment of the absorption for almost the whole wavelength range from 420 to 750 nm can be observed as the ICBA concentration is increased from 5 to 15 % wt. This is consistent with the hypothesis of a denser morphology giving rise to such an absorption increment, and in turn to a J_{SC} enhancement. The relation between morphology and V_{OC} will be discussed later. It should be pointed out that the J_{SC} variation is not the origin of the observed V_{OC} tuning effect, as will be proved later.

Fig.3 shows the dark *J-V* characteristics at room temperature for both concentrations of ICBA in a semilogarithmic representation. The circles correspond to the experimental values, the model curves are given as continuous lines. The model used consists of a general diode equation including resistance effects [39]

$$J = J_0\left[exp\left[\frac{q(V - JAR_S)}{nk_BT}\right] - 1\right] + \frac{V - JAR_S}{R_pA} \qquad (1)$$

where k_B is Boltzmann´s constant, T the temperature, A the active area of the device, R_P the parallel resistance describing the leakage of the junction at low voltage values and R_S is the series resistance attributed to the bulk and interfacial ohmic effects at relative high voltage region. Parameters n

and J_0 are the ideality factor and the saturation current density of the diode at medium voltage values, respectively. The values of n and J_0 depend on the current recombination mechanisms in the device [40]. It can be noted that the model fits very good to the experimental values at medium-high voltages, whereas for the low voltage region the model and the experimental curves deviates. That is attributed to hysteresis effects that will be discuss later in the text.

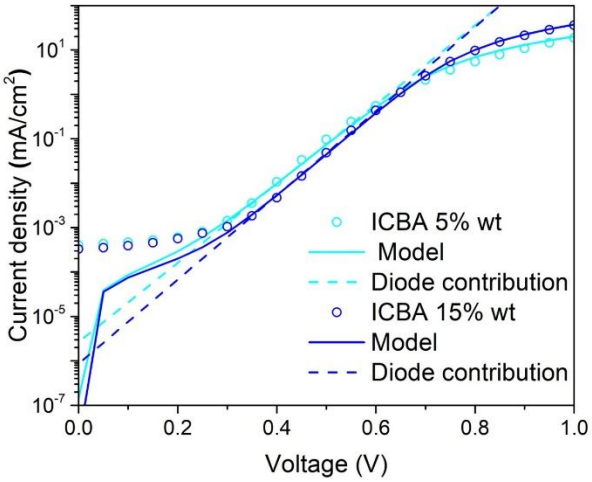

Figure 3. Experimental (circles) and modeled curves (continuous lines) at room temperature for the two different ICBA concentrations (see text). The dashed lines represent the contribution of the diode in both cases.

The dashed lines in Fig. 3 indicate the contribution of the modeled diode only. This diode contribution fits to the experimental quite well over the experimental linear region showing a good agreement between the modeled and the experimental dark current characteristics along the medium voltage region (0.3 V to 0.5 V) where the conduction mechanism described by the diode dominates (a further analysis about the fitting accuracy is available in the supplementary information). The values of the extracted parameters that model the experimental characteristic using Eq. 1 are reported in Table 2.

Table 2. Extracted parameters from dark *J-V-T* characteristics of both devices with different ICBA concentrations.

ICBA 5% wt					ICBA 15% wt				
T (K)	J_0 (1×10^{-6} mA/cm^2)	n	R_S (Ω•cm^2)	R_P (1×10^{6} Ω•cm^2)	T (K)	J_0 (1×10^{-6} mA/cm^2)	n	R_S (Ω•cm^2)	R_P (1×10^{5} Ω•cm^2)
294	2.66	1.91	11.40	1.47	294	0.66	1.76	5.61	8.95
303	3.64	1.9	11.40	2.36	303	1.33	1.75	4.39	6.51
313	7.64	1.89	8.95	3.17	313	2.99	1.73	3.66	1.38
323	12.60	1.86	7.33	3.34	323	7.14	1.72	2.68	2.85
333	26.60	1.84	5.70	3.50	333	14.10	1.70	2.27	1.71

The extracted values for R_S modeling the saturation region at high voltages are similar to those reported for binary PTB7-Th:$PC_{71}BM$ systems (2-15 Ω•cm^2) [41] and decreases for increasing

ICBA concentration which also explain the highest *FF* for 15% wt ICBA sample. Further, as expected, J_0 decreases as the concentration of ICBA increases, also according well to literature [16].

The J_0 and n values estimated from the solar cells under dark conditions (Fig.4) are used to predict the generated V_{OC} by devices under illumination using the following general relation:

$$V_{OC} = nk_BTln\left(\frac{J_{SC}}{J_0} + 1\right) \qquad (2)$$

This expression is derived from Eq. (1) at open circuit conditions. The calculated values for V_{OC} are: 0.73 V and 0.76 V for 5% and 15% ICBA concentration, respectively. The deviations between these values and the experimental ones (see Table 1) are not larger than 10 mV, which is well in the range of previous results [19]. Hence, this confirms that V_{OC} is practically determined by J_0 and n which are diode parameters related to recombination mechanisms occurring in both cases, in the dark and under illumination. This also confirms that the J_{SC} variation is not the origin of the observed V_{OC} tuning effect.

Aiming at the identification of the recombination mechanisms determining J_0, the *J-V-T* curves are modeled in order to analyze the temperature dependence of J_0 and of the ideality factor n [42, 43].

Fig.4 shows the experimental (circles) and modeled (continuous lines) characteristics *J-V-T* of the cells with the two different concentrations of ICBA. Operation temperatures above room temperature, i. e., for which charge collection is relatively constant [44, 45] are analyzed. The measurements are carried out at temperatures below 60 ℃ only due to the low melting point of the FM electrode (62 ℃). As expected, the current increases as the temperature increases.

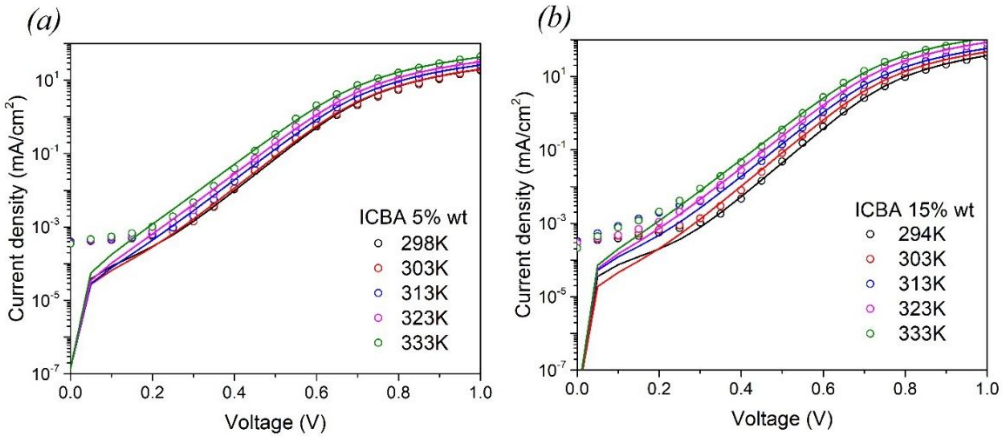

Figure 4. Dark *J-V-T* characteristics for TSCs with 5% wt (a) and 15% wt (b) ICBA concentrations. Experimental (circles) and modeled behavior (continuous line).

Note the almost perfect agreement of experimental data and the model above 0.3 V. For voltages below 0.3 V, a hysteresis phenomenon is observed. This low-voltage region usually is modeled by considering R_P[46, 22]. The hysteresis effect does not affect the linear diode region which is the region determining the V_{OC}. It should be noted that this hysteresis effect does not correspond to the one related with voltage scans but with a shift of the curve in the low-voltage region which is present even in measurements in one direction. This effect can be attributed to non-intentional ions at the device interfaces [47, 48].

First, by using the extracted parameters from dark J-V-T model curves and analyzing the dependance of an Arrhenius plot (J_0 and $1/k_BT$), the activation energies E_a are calculated as 0.55 eV and 0.66 eV for devices with 5% as 15% ICBA concentration, respectively. These calculated E_a values do not correspond to the gap energies of any of the materials (1.6 ,2.06, and 1.89 eV for PTB7-Th, ICBA and $PC_{71}BM$ respectively) [49,26,50] for band-to-band recombination. Also, these E_a values do not correspond to the half of the energy gab of the materials which would indicate recombination at the space charge region. Thus, classical recombination models are discarded [51]. Therefore, a modified Arrhenius plot including the ideality factor n is used

following the model proposed of Rau *et al* initially for inorganic heterojunctions [52] and validated for organic semiconductor heterojunctions [53] where the recombination mechanism is tunneling enhanced recombination. Thus, the activation energies E_a showed in Fig.5 are calculated using the following Eq. 3.

$$J_0 \propto exp\left[\frac{-E_a}{nkT}\right] \qquad (3)$$

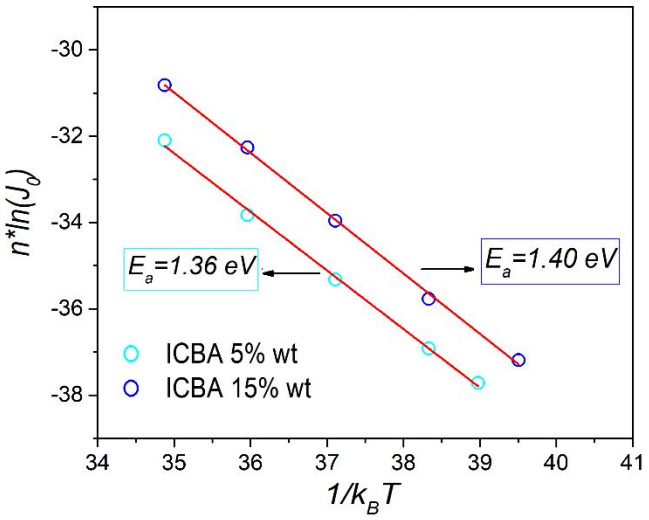

Figure 5. Modified Arrhenius plot for the temperature dependence of the reverse saturation current density and the ideality factor. The extracted E_a values are given for both ICBA concentrations. Inset: scheme of the main heterojunction indicating the calculated interface activation energies.

The activation energies are calculated as: $1.36 \pm 0.004\ eV$ and $1.40 \pm 0.001\ eV$ for devices with 5% as 15% ICBA concentration, respectively. Interestingly, the two activation energies deviate from each other by $0.04\ eV$ which nearly corresponds to the V_{OC} difference of $0.03\ V$ obtained for the two different ICBA concentrations. This result indicates that the variations of V_{OC} with the ICBA concentrations is caused by a variation in the activation energy of the charge carriers in the device. To get an accurate fitting, we emphasize it being necessary to address the following points: (i) to verify a good overlap between the diode contribution and the data as it is shown in Figs .S1a and c in the supplementary information; (ii) to fit the resistance regions. The error for the activation energies was calculated by considering the fitted error of such a diode region (see supplementary information).

A band diagram has been simulated to explore the relation between the activation energy and the main heterojunction (PTB7-Th:$PC_{71}BM$) interface. The diagram was calculated in thermal equilibrium using AFORS-HET [54] and is shown in Fig. 6. The parameters used for the simulation are included in Table S1 in the supplementary information. Note that the activation energies correspond to the difference between the Fermi level and the HOMO level of the PTB7-

Th (1.3 eV). This result is consistent with five binary bulk heterojunction solar cells for which different organic materials were used [40]. It should be mentioned that, although the simulation corresponds to a planar structure, it has been proven valid to explain interfacial phenomena and capacitance-voltage characteristics of bulk heterojunction solar cells [40].

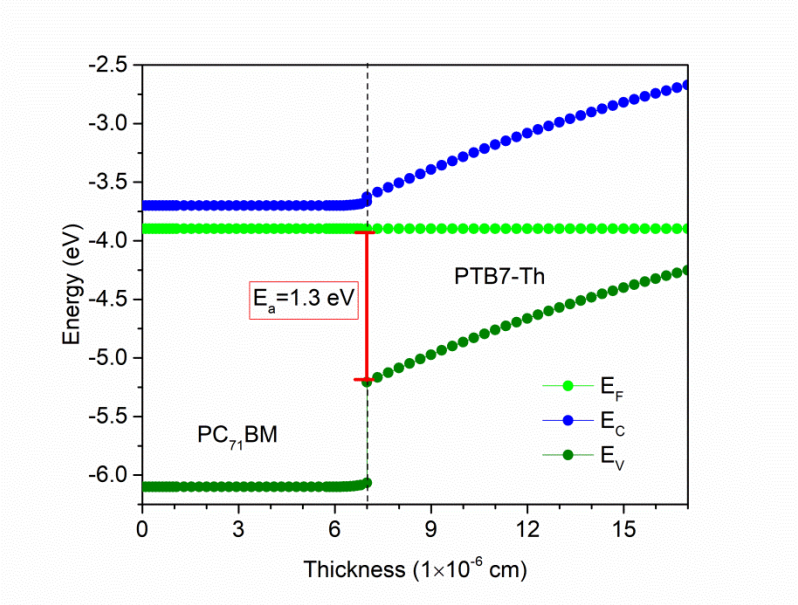

Figure 6. Simulated band diagram of the main device junction PTB7-Th:$PC_{71}BM$. Red line indicates the magnitude of the interfacial activation energy $E_a = E_F$(Fermi level) – E_V($HOMO_D$).

In the following, the origin of the variation of E_a with ICBA concentration will be discussed. Basically, as reported in literature, the V_{OC} tunning effect has been explained using two different approximations: i) molecular modifications such as mixed acceptor phase formations (known as an organic alloy approximation) and interfacial molecular substitutions [55, 56, 27,19]; and ii) modifications in the blend morphology [19]. In principle, the decrease of roughness for the high ICBA concentration and the measured absorbance indicate a modification in the blend morphology as the origin of the V_{OC} tuning in our samples. However, further compositional characterization should be performed since it has been reported that ICBA and $PC_{71}BM$ can form an alloy [55]. Eventually, both approximations suggest a variation of the HOMO level due to either compositional or morphological changes [19, 55]. This variation gives rise to a modification of the interface band gap or the lowest charge transfer energy (E_{CT}). This phenomenon is consistent with the relation $E_a = E_F - \mathrm{HOMO_D}$ obtained from the band diagram, where E_a can be considered as equivalent to E_{CT}. The equivalence between E_a and E_{CT} has been previously probed for binary organic solar cells [57]. Considering the present results and the linear relation between E_{CT} and V_{OC} reported for changes of E_{CT} when varying the ICBA concentration in a similar system [37, 19], we can infer that such an equivalence holds for ternary systems.

In summary, the simple method proposed here can be used not only to calculate the E_{CT} state for ternary solar cells indirectly, but also to determine the recombination mechanisms occurring in the solar cells under both dark and illumination conditions. This can be done since the measuring *J-V-T* conditions are similar to the operation ones of the solar cell, i.e., the flow of charge through the device in the diode region. Conversely, optical methods to determine E_{CT} rely on measurements at particular conditions, i. e., the low-intensity emission of some photons only.

CONCLUSION

Ternary bulk heterojunction organic solar cells based on PTB7-Th:$PC_{71}BM$:ICBA with two different low concentrations of the ICBA were fabricated and studied using *J-V-T* characteristics. The V_{OC} of the devices was consistent with the general V_{OC} equation depending on J_0 with an error of 1.38% and 1.33% for devices with an ICBA concentration of 5% wt and 15% wt, respectively. From *J-V-T* characteristics, the calculated interface activation energies using a modified Arrhenius type curve were E_a= 1.36 eV and 1.40 eV for devices with 5% wt and 15% wt ICBA concentration, respectively. A similar variation of these values was found with respect to the V_{OC} ones (0.72 V

and 0.75 V) for the two third component concentration. This confirms that the V_{OC} tuning effect observed in TSC's can be related to a variation of the activation energy of the charge carriers in the device. The recombination mechanism limiting the solar cells' J_0 and giving rise to such activation energies is tunneling-enhanced recombination. The activation energy values correspond to the difference between the Fermi level and the HOMO of the donor in a simulated band diagram. Finally, it is inferred that E_a and E_{CT} can be considered as being equivalent in the herein studied solar cells as it occurs in binary solar cells. Hence, the above results indicate that (i) tuning V_{OC} with a third component variation is an interfacial effect, (ii) our applied simple method can be used to study the V_{OC} tuning phenomena in ternary solar cells.

AUTHOR INFORMATION

Corresponding Author

* E-mail: janolasco@uv.mx

Present Addresses

O. Amargós-Reyes: Current postdoctoral fellow at Interdisciplinary Research Laboratory, ENES León, National Autonomous University of Mexico, 37684 León, Gto., Mexico.

Notes

The authors declare no competing financial interest.

ACKNOWLEDGMENT

Support given by CONACYT Mexico, Frontier Science 2019 project CF19-263955; UNAM PAPIIT TA101221, Mexico and by DAAD Germany, IVAC 2020, 57563946 is gratefully acknowledged. Amargós-Reyes thanks DGAPA post-doctoral fellowship (UNAM, Mexico). This work has been performed in the framework of the Bremen-Mexican Network on Sustainable Technologies for Environmental Applications (BreMex-STEAps.net).

REFERENCES

1. Sun, Y.; Liu, T.; Kan, Y.; Gao, K.; Tang, B.; Li, Y. Flexible Organic Solar Cells: Progress and Challenges. *Small Sci.* 2021, *1*, 2100001.

2. Lin, Y.; Magomedov, A.; Firdaus, Y.; Kaltsas, D.; El-Labban, A.; Faber, H.; Naphade, D. R.; Yengel, E.; Zheng, X.; Yarali, E.; Chaturvedi, N.; Loganathan, K.; Gkeka, D.; AlShammari, S. H.; Bakr, O. M.; Laquai, F.; Tsetseris, L.; Getautis, V.; Anthopoulos, T. D. 18.4 % Organic Solar Cells Using a High Ionization Energy Self-Assembled Monolayer as Hole-Extraction Interlayer. *ChemSusChem* 2021, *14*, 3569–3578.

3. Cui, Y.; Xu, Y.; Yao, H.; Bi, P.; Hong, L.; Zhang, J.; Zu, Y.; Zhang, T.; Qin, J.; Ren, J.; Chen, Z.; He, C.; Hao, X.; Wei, Z.; Hou, J. Single-Junction Organic Photovoltaic Cell with 19% Efficiency. *Adv. Mater.* 2021, *33*, 2102420.

4. Gao, K.; Miao, J.; Xiao, L.; Deng, W.; Kan, Y.; Liang, T.; Wang, C.; Huang, F.; Peng, J.; Cao, Y.; Liu, F.; Russell, T. P.; Wu, H.; Peng, X. Multi-Length-Scale Morphologies Driven by Mixed Additives in Porphyrin-Based Organic Photovoltaics. *Adv. Mater.* 2016, *28*, 4727–4733.

5. Gao, K.; Kan, Y.; Chen, X.; Liu, F.; Kan, B.; Nian, L.; Wan, X.; Chen, Y.; Peng, X.; Russell, T. P.; Cao, Y.; Jen, A. K. Y. Low-Bandgap Porphyrins for Highly Efficient Organic Solar Cells: Materials, Morphology, and Applications. *Adv. Mater.* **2020**, *32* , 1906129.

6. Gong, Y.; Kan, Z.; Xu, W.; Wang, Y.; AlShammari, S. H.; Laquai, F.; Lai, W. Y.; Huang, W. Wide-Bandgap Small Molecular Acceptors Based on a Weak Electron-Withdrawing Moiety for Efficient Polymer Solar Cells. *Sol. RRL* **2018**, *2*, 1800120.

7. Gasparini, N.; Salleo, A.; McCullonch, I.; Baran, D. The Role of the Third Component in Ternary Organic Solar Cells. *Nat. Rev. Mater.* **2019**, *4*, 229–242.

8. Huang, H.; Yang, L.; Sharma, B. Recent Advances in Organic Ternary Solar Cells. *J. Mater. Chem. A.* **2017**, *5*, 11501–11517.

9. Wang, Y.; Xu, W.; Yi, J.; Zuo, C.; Gong, Y.; Liu, Y.; Lai, W. Y.; Huang, W. Improving the Exciton Dissociation of Polymer/Fullerene Interfaces with a Minimal Loading Amount of Energy Cascading Molecular Dopant. *J. Mater. Chem. A.* **2018**, *6*, 15977–15984.

10. Wang, Y.; Xu, W. D.; Zhang, J. D.; Zhou, L.; Lei, G.; Liu, C. F.; Lai, W. Y.; Huang, W. A Small Molecule/Fullerene Binary Acceptor System for High-Performance Polymer Solar Cells with Enhanced Light-Harvesting Properties and Balanced Carrier Mobility. *J. Mater. Chem. A* **2017**, *5*, 2460–2465.

11. An, Q.; Zhang, F.; Zhang, J.; Tang, W.; Deng, Z.; Hu, B. Versatile Ternary Organic Solar Cells: A Critical Review. *Energy Environ. Sci.* **2016**, *9*, 281–322.

12. Cheng, P.; Yan, C.; Wu, Y.; Wang, J.; Qin, M.; An, Q.; Cao, J. Alloy Acceptor%: Superior Alternative to PCBM toward Effi Cient and Stable Organic Solar Cells. *Adv. Mater.* **2016**, *28,* 8021–8028.

13. Khlyabich, P. P.; Sezen-edmonds, M.; Howard, J. B.; Thompson, B. C. Formation of Organic Alloys in Ternary-Blend Solar Cells with Two Acceptors Having Energy- Level O Ff Sets Exceeding 0.4 EV. *ACS Energy Lett.* **2017**, *2*, 2149–2156.

14. Huang, J.; Velusamy, M.; Ho, K.; Lin, J.; Chu, C. A Ternary Cascade Structure Enhances the Efficiency of Polymer Solar Cells. *J. Mater. Chem.* **2010**, *20*, 2820–2825.

15. Xu, W.; Wu, B.; Zheng, F.; Yang, X.; Jin, H.; Zhu, F.; Hao, X. Förster Resonance Energy Transfer and Energy Cascade in Broadband Photodetectors with Ternary Polymer Bulk Heterojunction. *J. Phys. Chem.* **2015**, *119*, 21913–219120.

16. Li, H.; Zhang, Z.; Li, Y.; Wang, J. Tunable Open-Circuit Voltage in Ternary Organic Solar Cells. *Appl. Phys. Lett.* **2012**, *101*, 163302.

17. Lee, M. A Machine Learning – Based Design Rule for Improved Open-Circuit Voltage in Ternary Organic Solar Cells. *Adv. Intell. Syst.* **2020**, *2*, 1900108.

18. Lami, V.; Hofstetter, Y. J.; Butscher, J. F.; Vaynzof, Y. Energy Level Alignment in Ternary Organic Solar Cells. *Adv. Electron. Mater.* **2020**, *6*, 2000213.

19. Mollinger, S. A.; Vandewal, K.; Salleo, A. Microstructural and Electronic Origins of Open-Circuit Voltage Tuning in Organic Solar Cells Based on Ternary Blends. *Adv. Energy Mater.* **2015**, *5*, 1501335.

20. Lami, V.; Weu, A.; Zhang, J.; Friend, R. H.; Lami, V.; Weu, A.; Zhang, J.; Chen, Y.; Fei, Z.; Heeney, M. Visualizing the Vertical Energetic Landscape in Organic Photovoltaics

Visualizing the Vertical Energetic Landscape in Organic Photovoltaics. *Joule* **2019**, *3*, 2513–2534.

21. Olthof, S. The Impact of UV Photoelectron Spectroscopy on the Field of Organic Optoelectronics — A Retrospective. *Adv. Opt. Mater.* **2021**, *9*, 2100227.

22. Vandewal, K. Interfacial Charge Transfer States in Condensed Phase Systems. *Annu. Rev. Phys. Chem.* **2016**, *67*, 113–133.

23. Nolasco, J. C.; Ramos-Ortiz, G.; Maldonado, J. L.; Barbosa-Garcia, O.; Ecker, B.; Von Hauff, E. Polymer/Cathode Interface Barrier Limiting the Open Circuit Voltage in Polymer:Fullerene Organic Bulk Heterojunction Solar Cells: A Quantitative Analysis. *Appl. Phys. Lett.* **2014**, *104*, 043308.

24. Amargós-Reyes, O.; Caballero-Quintana, I.; Maldonado, J.-L.; Nicasio-Collazo, J.; Romero-Borja, D. Single Graphene Derivative Layer as a Hole Transport in Organic Solar Cells Based on PBDB-T:ITIC. *Appl. Opt.* **2020**, *59*, 8285–8292.

25. Caballero-Quintana, I.; Romero-Borja, D.; Maldonado, J. L.; Nicasio-Collazo, J.; Amargós-Reyes, O.; Jiménez-González, A. Interfacial Energetic Level Mapping and Nano-Ordering of Small Molecule/Fullerene Organic Solar Cells by Scanning Tunneling Microscopy and Spectroscopy. *Nanomaterials* **2020**, *10*, 427.

26. He, Y.; Chen, H.; Hou, J.; Li, Y. Indene - C 60 Bisadduct%: A New Acceptor for High-Performance Polymer Solar Cells. *J. Am. Chem. Soc.* **2010**, *132*, 1377–1382.

27. Khlyabich, P. P.; Burkhart, B.; Thompson, B. C. Efficient Ternary Blend Bulk Heterojunction Solar Cells with Tunable. *J. Am. Chem. Soc.* **2011**, *133*, 14534–14537.

28. Gong, Y.; Zhang, J.; Du, B.; Wang, M.; Lai, W. Y.; Huang, W. Design, Synthesis, and Postvapor Treatment of Neutral Fulleropyrrolidine Electron-Collecting Interlayers for High-Efficiency Inverted Polymer Solar Cells. *ACS Appl. Electron. Mater.* **2019**, *1*, 854–861.

29. Cheng, P.; Li, Y.; Zhan, X. Efficient Ternary Blend Polymer Solar Cells with Indene-C60 Bisadduct as an Electron-Cascade Acceptor. *Energy Environ. Sci.* **2014**, *7*, 2005–2011.

30. Sharma, R.; Lee, H.; Gupta, V.; Kim, H.; Kumar, M.; Sharma, C.; Chand, S.; Yoo, S.; Gupta, D. Photo-Physics of PTB7, PCBM and ICBA Based Ternary Solar Cells. *Org. Electron.* **2016**, *34*, 111–117.

31. Snaith, H. J. How Should You Measure Your Excitonic Solar Cells? *Energy Environ. Sci.* **2012**, *5*, 6513–6520.

32. Pérez-Gutiérrez, E.; Barreiro-Argüelles, D.; Maldonado, J. L.; Meneses-Nava, M. A.; Barbosa-García, O.; Ramos-Ortíz, G.; Rodríguez, M.; Fuentes-Hernández, C. Semiconductor Polymer/Top Electrode Interface Generated by Two Deposition Methods and Its Influence on Organic Solar Cell Performance. *ACS Appl. Mater. Interfaces* **2016**, *8*, 28763–28770.

33. Montoya, D. M.; Pérez-Gutiérrez, E.; Barbosa-Garcia, O.; Bernal, W.; Maldonado, J. L.; Percino, M. J.; Meneses, M. A.; Cerón, M. Defects at the Interface Electron Transport Layer and Alternative Counter Electrode, Their Impact on Perovskite Solar Cells Performance. *Sol. Energy* **2020**, *195*, 610–617.

34. Lu, L.; Kelly, M. A.; You, W.; Yu, L. Status and Prospects for Ternary Organic Photovoltaics. *Nat. Publ. Gr.* **2015**, *9*, 491–500.

35. Sun, Y.; Li, G.; Wang, L.; Huai, Z.; Fan, R.; Huang, S.; Fu, G.; Yang, S. Solar Energy Materials and Solar Cells Simultaneous Enhancement of Short-Circuit Current Density, Open Circuit Voltage and Fill Factor in Ternary Organic Solar Cells Based on PTB7-Th: IT-. *Sol. Energy Mater. Sol. Cells* **2018**, *182*, 45–51.

36. Shi, Y.; Fu, J.; Ji, Z. Efficient Ternary Polymer Solar Cells by Doping Fullerene Derivatives. *Thin Solid Films* **2017**, *636*, 20–25.

37. Peng, Z.; Xia, Y.; Gao, F.; Xiong, K.; Hu, Z.; James, I. .; Chen, J.; Wang, E.; Hou, L. Dual Ternary System for Highly Efficient ITO-Free Inverted Polymer Solar Cells†. *J. Mater. Chem. A* **2015**, *3*, 18365–18371.

38. Wang, Z.; Gao, K.; Kan, Y.; Zhang, M.; Qiu, C.; Zhu, L.; Zhao, Z.; Peng, X.; Feng, W.; Qian, Z.; Gu, X.; Jen, A. K. Y.; Tang, B. Z.; Cao, Y.; Zhang, Y.; Liu, F. The Coupling and Competition of Crystallization and Phase Separation, Correlating Thermodynamics and Kinetics in OPV Morphology and Performances. *Nat. Commun.* **2021**, *12*, 332.

39. Luque, A.; Hegedus, S. *Handbook of Photovoltaic Science and Engineering*, 2nd ed.; Wiley, Hoboken, NJ, 2011.

40. Nolasco, J. C.; Castro-Carranza, A.; León, Y. A.; Briones-Jurado, C.; Gutowski, J.; Parisi, J. Understanding the Open Circuit Voltage in Organic Solar Cells on the Basis of a Donor-Acceptor Abrupt (p-n++) Heterojunction. *Sol. Energy* 2019, *184*, 610–619.

41. Amargós-Reyes, O.; Maldonado, J.L.; Romero-Borja, D.; Barreiro-Argüelles, D.; Caballero-Quintana, I.; Barbosa-García, O.; Gaspar, A. J. Organic Photovoltaic Cell Analysis through Quantum Efficiency and Scanning Tunneling Microscopy of the Donor / Blend as an Active Film. *J. Mater. Sci.* 2019, *54*, 2427–2445.

42. Tvingstedt, K.; Deibel, C. Temperature Dependence of Ideality Factors in Organic Solar Cells and the Relation to Radiative Efficiency. *Adv. Energy Mater.* 2016, *6*, 1502230.

43. You, A.; Be, M. A. Y.; In, I. Recombination Mechanisms in Amorphous Silicon / Crystalline Silicon Heterojunction Solar Cells. *J. Appl. Phys.* 2000, *87*, 2639–2645.

44. Hormann, U.; Kraus, J.; Mark, G.; Christoph, S.; Theresa, L.; Stefan, G.; Stephan, K.; Klein, K.; Stutzman, M.; Hubert J, K.; Wolfgang, B. Quantification of Energy Losses in

Organic Solar Cells from Temperature-Dependent Device Characteristics. *Phys. Rev. B* **2013**, *88*, 235307.

45. Riedel, B. I.; von Hauff, E.; Parisi, J.; Martín, N.; Giacalone, F.; Dyakonov, V. Diphenylmethanofullerenes%: New and Efficient Acceptors in Bulk-Heterojunction Solar Cells **. *Adv. Funct. Mater.* **2005**, *15*, 1979–1987.

46. Nolasco, J. C.; Cabré, R.; Ferré-Borrull, J.; Marsal, L. F.; Estrada, M.; Pallarès, J. Extraction of Poly (3-Hexylthiophene) (P3HT) Properties from Dark Current Voltage Characteristics in a P3HT/ n -Crystalline-Silicon Solar Cell. *J. Appl. Phys.* **2010**, *107*, 044505.

47. Nguyen, P. H.; Scheinert, S.; Berleb, S.; Bruttig, W.; Paasch, G. The Infuence of Deep Traps on Transient Current- Voltage Characteristics of Organic Light-Emitting Diodes. *Org. Electron.* **2001**, *2*, 105–120.

48. Zhang, C.; Tong, S. W.; Zhu, C.; Jiang, C.; Kang, E. T.; Zhang, C.; Tong, S. W.; Zhu, C.; Jiang, C.; Kang, E. T. Enhancement in Open Circuit Voltage Induced by Deep Interface Hole Traps in Polymer-Fullerene Bulk Heterojunction Solar Cells Enhancement in Open

Circuit Voltage Induced by Deep Interface Hole Traps in Polymer-Fullerene Bulk Heterojunction Solar Cells. *Appl Phys. Lett.* **2009**, *94*, 103305.

49. Xiao, B.; Zhao, Y.; Tang, A.; Wang, H.; Yang, J.; Zhou, E. PTB7-Th Based Organic Solar Cell with a High Voc of 1.05 V by Modulating the LUMO Energy Level of Benzotriazole-Containing Non-Fullerene Acceptor. *Sci. Bull.* **2017**, *62*, 1275–1282.

50. He, Y.; Li, Y. Fullerene Derivative Acceptors for High Performance Polymer Solar Cells. *Phys. Chem. Chem. Phys.* **2011**, *13*, 1970–1983.

51. Marsal, L. F.; Martin, I.; Pallares, J.; Orpella, A.; Alcubilla, R. Annealing Effects on the Conduction Mechanisms of P+ -Amorphous- Si0.8C0.2:H/n-Crystalline-Si Diodes. *J. Appl. Phys.* **2003**, *94*, 2622–2626.

52. Rau, U.; Jasenek, A.; Schock, H. W.; Engelhardt, F.; Meyer, T. Electronic Loss Mechanisms in Chalcopyrite Based Heterojunction Solar Cells. *Thin Solid Films,* **2000**, *361–362*, 298–302.

53. Nolasco, J. C.; Marsal, L. F.; Palomares, E. Relation between the Barrier Interface and the Built-in Potential in Pentacene/C 60 Solar Cell. *Appl. Phys. Lett.* **2010**, *97*, 013305.

54. Varache, R.; Leendertz, C.; Gueunier-Farret, M. E.; Haschke, J.; Muñoz, D.; Korte, L. Investigation of Selective Junctions Using a Newly Developed Tunnel Current Model for Solar Cell Applications. *Sol. Energy Mater. Sol. Cells* **2015**, *141*, 14–23. https://doi.org/10.1016/j.solmat.2015.05.014.

55. Street, R. A.; Davies, D.; Khlyabich, P. P.; Burkhart, B.; Thompson, B. C. Origin of the Tunable Open-Circuit Voltage in Ternary Blend Bulk Heterojunction Organic Solar Cells. *J. Am. Chem. Soc.* **2013**, *135*, 986–989.

56. Angmo, D.; Bjerring, M.; Nielsen, N. C.; Thompson, B. C.; Krebs, F. C. Fullerene Alloy Formation and the Benefits for Efficient Printing of Ternary Blend Organic Solar Cells. *J. Mater. Chem. C* **2015**, *3*, 5541–5548.

57. Hormann, U.; Kraus, J.; Mark, G.; Christoph, S.; Theresa, L.; Stefan, G.; Stephan, K.; Klein, K.; Stutzman, M.; Hubert J, K.; Wolfgang, B. Quantification of Energy Losses in Organic Solar Cells from Temperature-Dependent Device Characteristics. *Phys. Rev. B* **2013**, *88*, 235307.

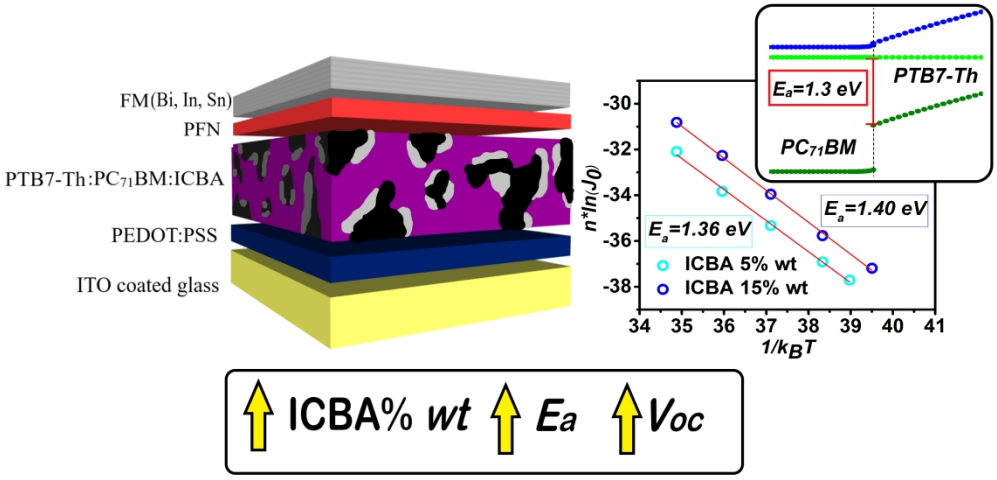

Graphical abstract

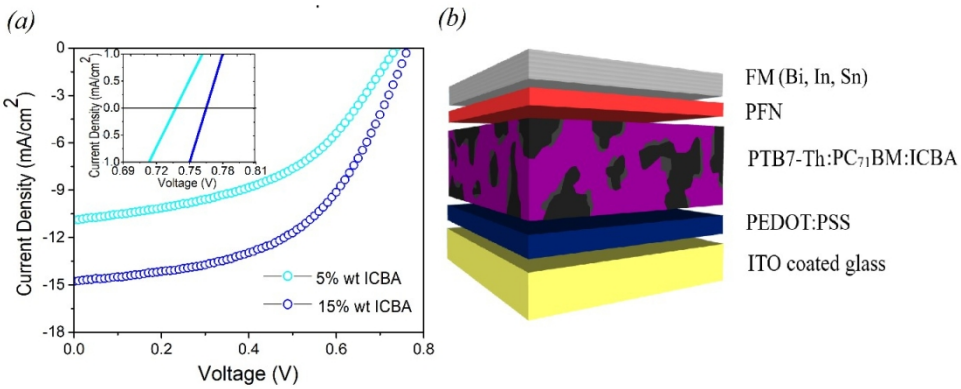

Figure 1. (a) J-V characteristics under illumination for TSC's with both 5% wt or 15% wt ICBA concentrations. The inset is showing a zoom in of the increment of the VOC got by increasing the ICBA concentration in the ternary blend. (b) TSCs device structure where ICBA domains are shown to be at the interfaces between the main donor:acceptor interface.

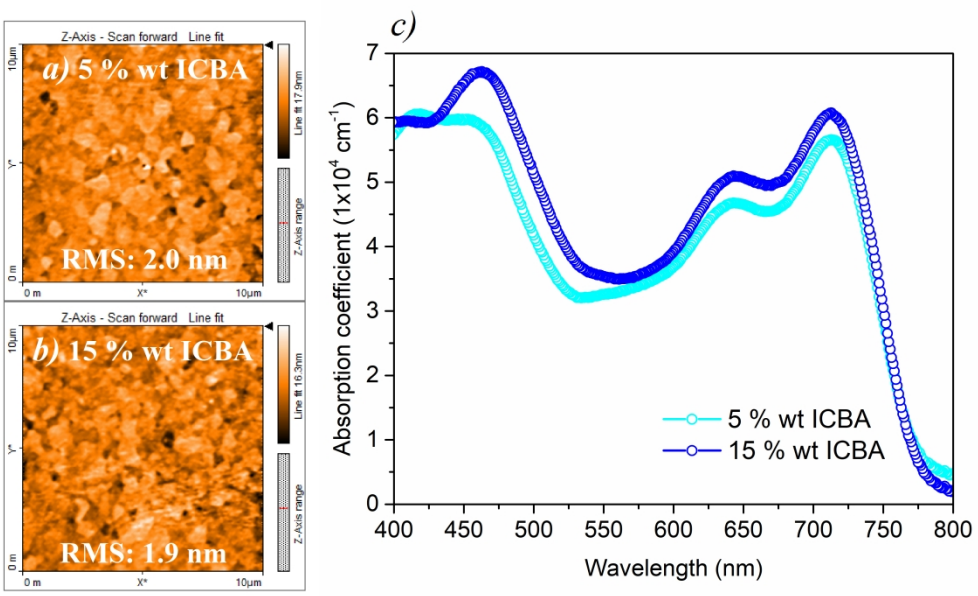

Figure 2

1037x646mm (96 x 96 DPI)

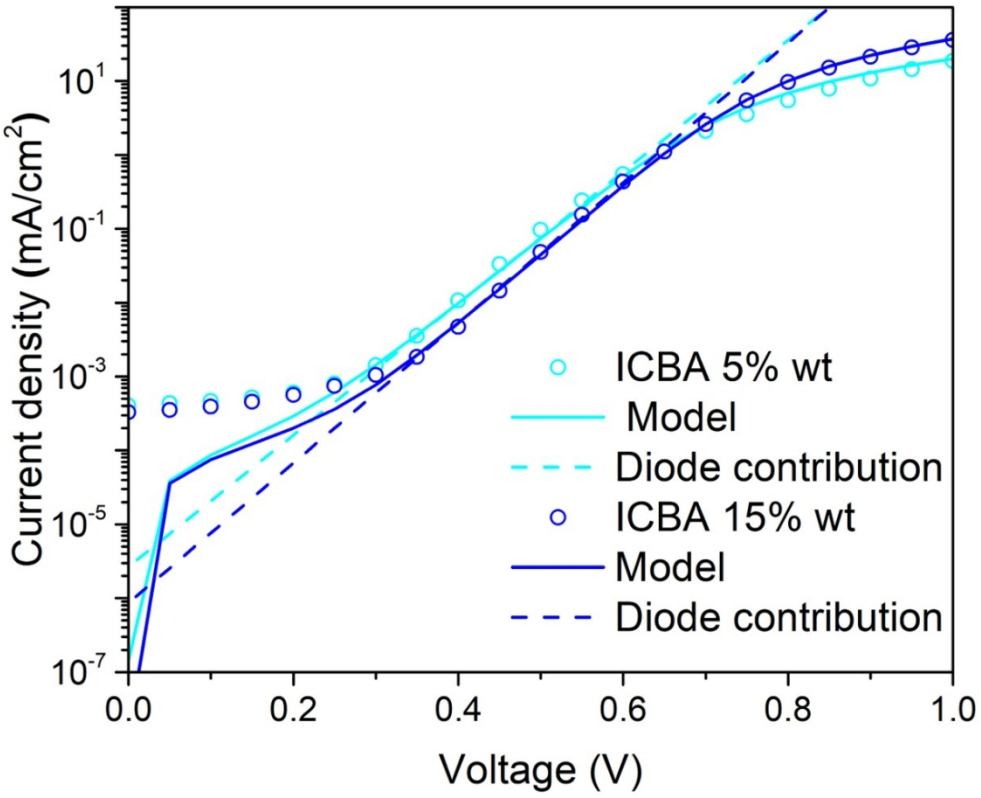
Current density (mA/cm^2)
10^{1}
10^{-1}
10^{-3}
10^{-5}
10^{-7}
0.0
0.2
0.4
0.6
0.8
1.0
Voltage (V)
ICBA 5% wt
Model
Diode contribution
ICBA 15% wt
Model
Diode contribution

Figure 3

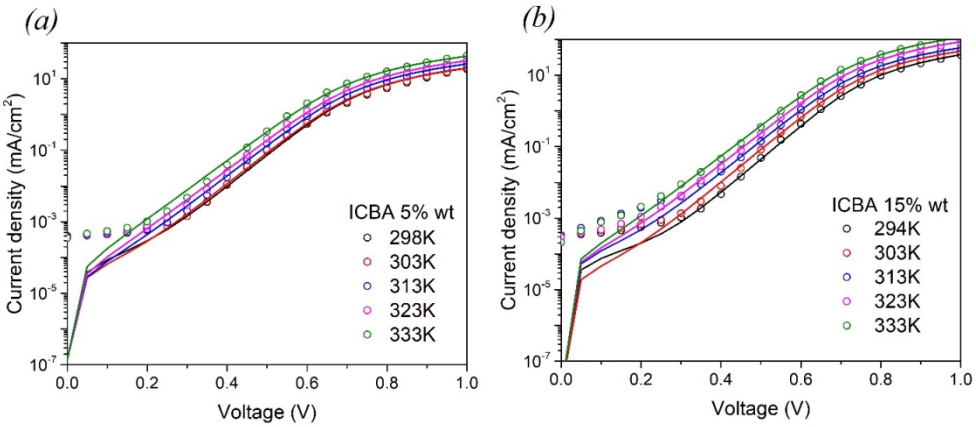
(a)
Current density (mA/cm^2)
Voltage (V)
ICBA 5% wt
298K
303K
313K
323K
333K
(b)
Current density (mA/cm^2)
Voltage (V)
ICBA 15% wt
294K
303K
313K
323K
333K

Figure 4

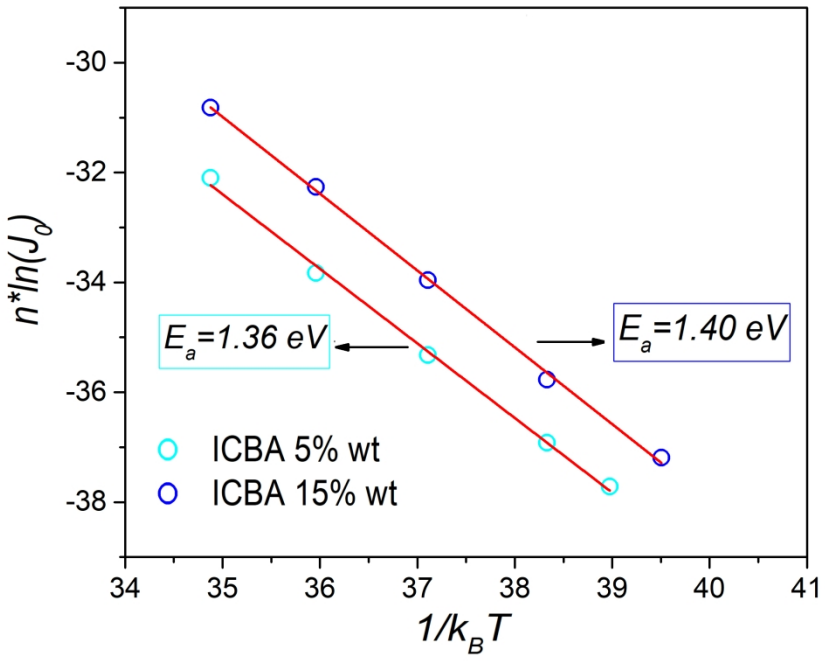
-30
-32
-34
-36
-38
34
35
36
37
38
39
40
41
n*ln(J0)
1/kBT
Ea=1.36 eV
Ea=1.40 eV
ICBA 5% wt
ICBA 15% wt

Figure 5

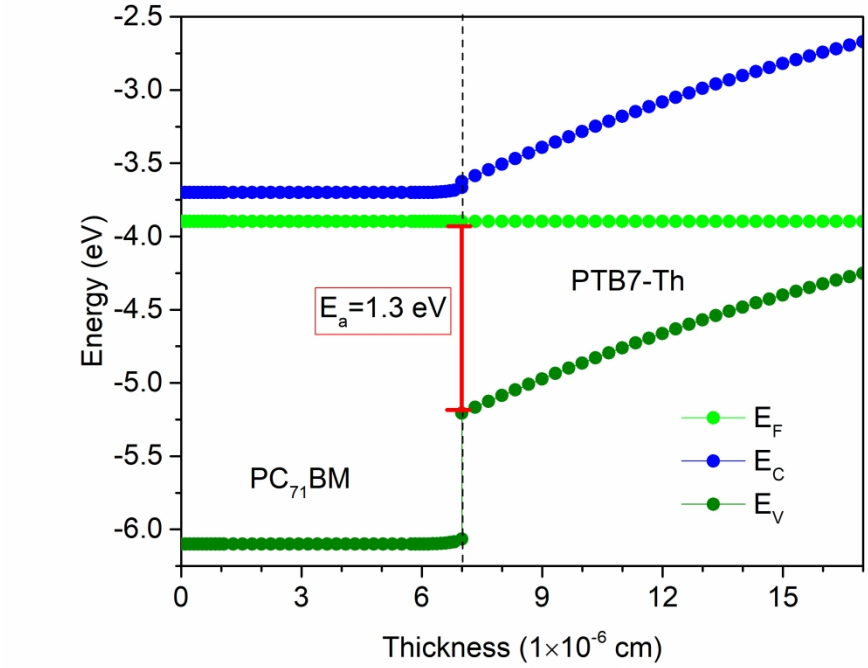

Figure 6

272x208mm (300 x 300 DPI)